8-2023

Improved Fine-Scale Tropical Forest Cover Mapping for Southeast Asia Using Planet-NICFI and Sentinel-1 Imagery

Feng Yang

Xin Jiang

Alan D. Ziegler

Lyndon Estes

Jin Wu

See next page for additional authors

Authors

Feng Yang, Xin Jiang, Alan D. Ziegler, Lyndon Estes, Jin Wu, Anping Chen, and Philippe Ciais

Journal of Remote Sensing
A SCIENCE PARTNER JOURNAL

RESEARCH ARTICLE

Improved Fine-Scale Tropical Forest Cover Mapping for Southeast Asia Using Planet-NICFI and Sentinel-1 Imagery

Feng Yang[1], Xin Jiang[1], Alan D. Ziegler[2], Lyndon D. Estes[3], Jin Wu[4,5], Anping Chen[6], Philippe Ciais[7], Jie Wu[1], and Zhenzhong Zeng[1*]

[1]School of Environmental Science and Engineering, Southern University of Science and Technology, Shenzhen 518055, China. [2]Faculty of Fisheries Technology and Aquatic Resources, Mae Jo University, Chiang Mai, Thailand. [3]Graduate School of Geography, Clark University, Worcester, MA, USA. [4]School for Biological Sciences and Institute for Climate and Carbon Neutrality, The University of Hong Kong, Hong Kong, China. [5]State Key Laboratory of Agrobiotechnology, The Chinese University of Hong Kong, Shatin, Hong Kong, China. [6]Department of Biology and Graduate Degree Program in Ecology, Colorado State University, Fort Collins, CO 80523, USA. [7]Laboratoire des Sciences du Climat et de l'Environnement, UMR 1572 CEA-CNRS-UVSQ, Gif-sur-Yvette, France.

*Address correspondence to: zengzz@sustech.edu.cn

Citation: Yang F, Jiang X, Ziegler AD, Estes LD, Wu J, Chen A, Ciais P, Wu J, Zeng Z. Improved Fine-Scale Tropical Forest Cover Mapping for Southeast Asia Using Planet-NICFI and Sentinel-1 Imagery. *J. Remote Sens.* 2023;3:Article 0064. https://doi.org/10.34133/remotesensing.0064

Submitted 30 January 2023
Accepted 24 July 2023
Published 10 August 2023

The accuracy of existing forest cover products typically suffers from "rounding" errors arising from classifications that estimate the fractional cover of forest in each pixel, which often exclude the presence of large, isolated trees and small or narrow forest clearings, and is primarily attributable to the moderate resolution of the imagery used to make maps. However, the degree to which such high-resolution imagery can mitigate this problem, and thereby improve large-area forest cover maps, is largely unexplored. Here, we developed an approach to map tropical forest cover at a fine scale using Planet and Sentinel-1 synthetic aperture radar (SAR) imagery in the Google Earth Engine platform and used it to map all of Southeastern Asia's forest cover. The machine learning approach, based on the Random Forests models and trained and validated using a total of 37,345 labels collected from Planet imagery across the entire region, had an accuracy of 0.937 and an F1 score of 0.942, while a version based only on Planet imagery had an accuracy of 0.908 and F1 of 0.923. We compared the accuracy of our resulting maps with 5 existing forest cover products derived from medium-resolution optical-only or combined optical-SAR approaches at 3,000 randomly selected locations. We found that our approach overall achieved higher accuracy and helped minimize the rounding errors commonly found along small or narrow forest clearings and deforestation frontiers where isolated trees are common. However, the forest area estimates varied depending on topographic location and showed smaller differences in highlands (areas >300 m above sea level) but obvious differences in complex lowland landscapes. Overall, the proposed method shows promise for monitoring forest changes, particularly those caused by deforestation frontiers. Our study also represents one of the most extensive applications of Planet imagery to date, resulting in an open, high-resolution map of forest cover for the entire Southeastern Asia region.

Introduction

Accurate assessment of tree cover is crucial for managing and conserving tropical forests, which play a vital role in protecting watersheds and mitigating climate change, in addition to being the world's most important reservoirs of biodiversity and the key source of livelihoods in many areas of the world [1–7]. A variety of natural and anthropogenic phenomena contribute to high annual rates of tropical forest loss, including logging, conversion to other land uses (agriculture, mining, reservoirs, etc.), mass wasting, storm damage, wildfires, disease, and extreme droughts [8–12]. Forests also regenerate naturally or through various types of forest rehabilitation and management activities. Since the early 21st century, the expansion of agriculture has caused dramatic forest cover losses in the Southeast Asia (SEA) [9,13]. However, recent studies diverge substantially in their estimates of how much tropical forest for SEA remains [14–16]. For example, the estimates of forest cover in 10 SEA countries range from 2.085 to 3.494 million ha [9,16–22]. The differences in these estimates arise from the different mapping approaches used in the assessments, as well as the spatial scale of assessment.

Studies mapping the extent of tropical forests typically rely on a single type of remote sensing data, relying entirely on either

optical imagery [9,23,24], synthetic aperture radar (SAR) [16,25,26], or lidar [27]. Efforts based on optical sensors have primarily resulted in medium- to coarse-resolution forest cover datasets [28], such as the ≥1-km resolution products of the Advanced Very High-Resolution Radiometer (AVHRR; [29,30]), a variety of ≥100-m resolution products developed from the Moderate Resolution Imaging Spectroradiometer (MODIS), Visible Infrared Imaging Radiometer Suite (VIIRS), or PROBA-V ([31,32]), and ≥25-m resolution products based on Sentinel-2, Landsat, and/or SPOT [9,24]. Only recently have 3 comprehensive forest maps been produced either using higher-resolution (10 m) optical imagery or based on a mix of optical and SAR sensors [20,33,34].

While these recent products demonstrate that advances in remote sensing technology have greatly improved the ability to map the extent and dynamics of forest cover changes, substantial uncertainty remains due to several factors. One source of uncertainty is the criteria used to define a forest, which can lead to large differences in forest area estimates [14,15,35,36]. Another major source relates to errors in classifying land cover types at the level of individual pixels [15,35,37–41]. Moderate- to coarse-resolution tropical forest cover maps have large uncertainties within heterogeneous landscapes [14,15,29,42], while products made using finer-resolution sensors can still contain image contamination errors caused by clouds and smog, which also lead to classification error [43–46]. Although the classification errors are bidirectional, with forest classified as non-forest and vice versa, the aggregate error can be substantial in fragmented and complex landscapes, as referred to as "rounding" error, which poses a major challenge for monitoring changes in forest area and boundaries arising from a variety of contemporary activities that cause small-scale forest loss, such as selected/illegal logging, swidden/fallow farming, and the gradual encroachment of permanent fields into adjacent forests [11,47,48]. These particular activities tend to produce geometrically irregular patches of land cover that are often smaller than the pixel resolution (e.g., 25 to 30 m) of the most readily available remote sensing products [11,14,29,37].

The uncertainties in forest cover estimates are therefore fundamentally a problem of remote sensing, as they are largely attributable to the characteristics of sensors, particularly their spatial and temporal resolution. The sensor's spatial resolution is mainly responsible for rounding errors, as it controls how well small-scale forest features can be detected, while temporal resolution (interval) determines whether a sufficient number of clear images are available to generate consistent, contemporaneous coverage over large areas, which is difficult in cloudy regions [49]. These 2 dimensions were traditionally in tension with one another, as gains in one typically require sacrifice in the other. However, this trade-off is increasingly being circumvented by using a larger number of satellites, which enable higher revisitation rates from lower orbits. The most prominent example is the fleet of >200 satellites operated by Plane, which captures daily <5-m resolution optical imagery [50]. Although commercial, Norway's International Climate & Forests Initiative (NICFI) has made Planet's 4.77-m and semiannual analysis-ready mosaics covering the world's tropics publicly available at no cost (https://www.planet.com/nicfi/). The spatial resolution of these products offers the promise of reducing rounding errors, while the daily frequency helps to increase the number of clear observations within a defined period, thereby minimizing the uncertainty caused by atmospheric contamination [51]. However, the degree to which such high spatiotemporal resolution optical data can reduce map error has not been fully explored, given that a thorough assessment requires investigation over large spatial extents and across a broad diversity of forest conditions, which has only now become possible with the release of the NICFI data.

To answer this question, we developed a machine-learning approach for mapping forest cover within the Google Earth Engine (GEE) platform [52], which combines Planet NICFI imagery along with C-band SAR imagery captured by Sentinel-1 C-band at near-high resolution (10 m) [53], and used it to map all of SEA's forests at ~5-m resolution. Our goal was to develop a dataset that enables a thorough investigation of the extent to which increased image resolution can reduce the rounding error problem, and create in the future a new product for monitoring tropical forest dynamics in a region experiencing rapid forest change. Combining these 2 different image sources allowed us to first investigate whether high-resolution optical data are sufficient on its own to reduce forest cover classification errors, or whether SAR, with its relative insensitivity to atmospheric conditions and greater sensitivity to vegetational structural aspects such as height [16], provides additional information needed to most effectively minimize error. The answer to this latter question is not certain, and therefore of broad interest, as other dual-sensor land cover mapping studies (e.g., for crop types) have shown that SAR often does little to improve classification accuracy relative to multi-spectral optical data (e.g., [54,55]). To examine the degree to which our new, high-resolution maps improved on previous products, we compared the accuracy of our maps with several forest cover maps drawn from existing products. We further evaluated how forest cover estimates derived from our maps compare to those developed from other products, assessing differences at the level of individual countries, and between different topographic regions (highland versus lowland), to more fully examine how rounding errors propagate into inventory uncertainties. We also estimated how fractional cover varies with the decreasing resolution, to more fully understand the connection between resolution and rounding errors.

Our study provides new insight into how well the growing availability of high spatiotemporal resolution remote sensing can resolve a major source of error in land cover mapping, within the context of one of the most extensive applications of the newly available Planet data that have been undertaken to date. Our approach builds on recent efforts by the Earth observation community to combine SAR and optical imagery to improve forest cover detection and classification (e.g., [15,20,28,48]).

Methods

Study area

SEA contains about 15% of the world's tropical forests and is an important hotspot for global biodiversity and carbon storage [4]. Spanning a land area of 4.5 million km^2, this region is composed of 11 countries (Fig. 1): Brunei, Cambodia, Lao PDR, Myanmar, Philippines, Thailand, Timor Leste, Vietnam, Singapore, Malaysia, and Indonesia. Of them, Cambodia, Lao PDR, Myanmar, Thailand, and Vietnam belong to the Greater Mekong Subregion (https://greatermekong.org/), while the other countries are largely maritime with wetter climates. This region extends over the longitude–latitude domain of 92.19° to 141.02°E

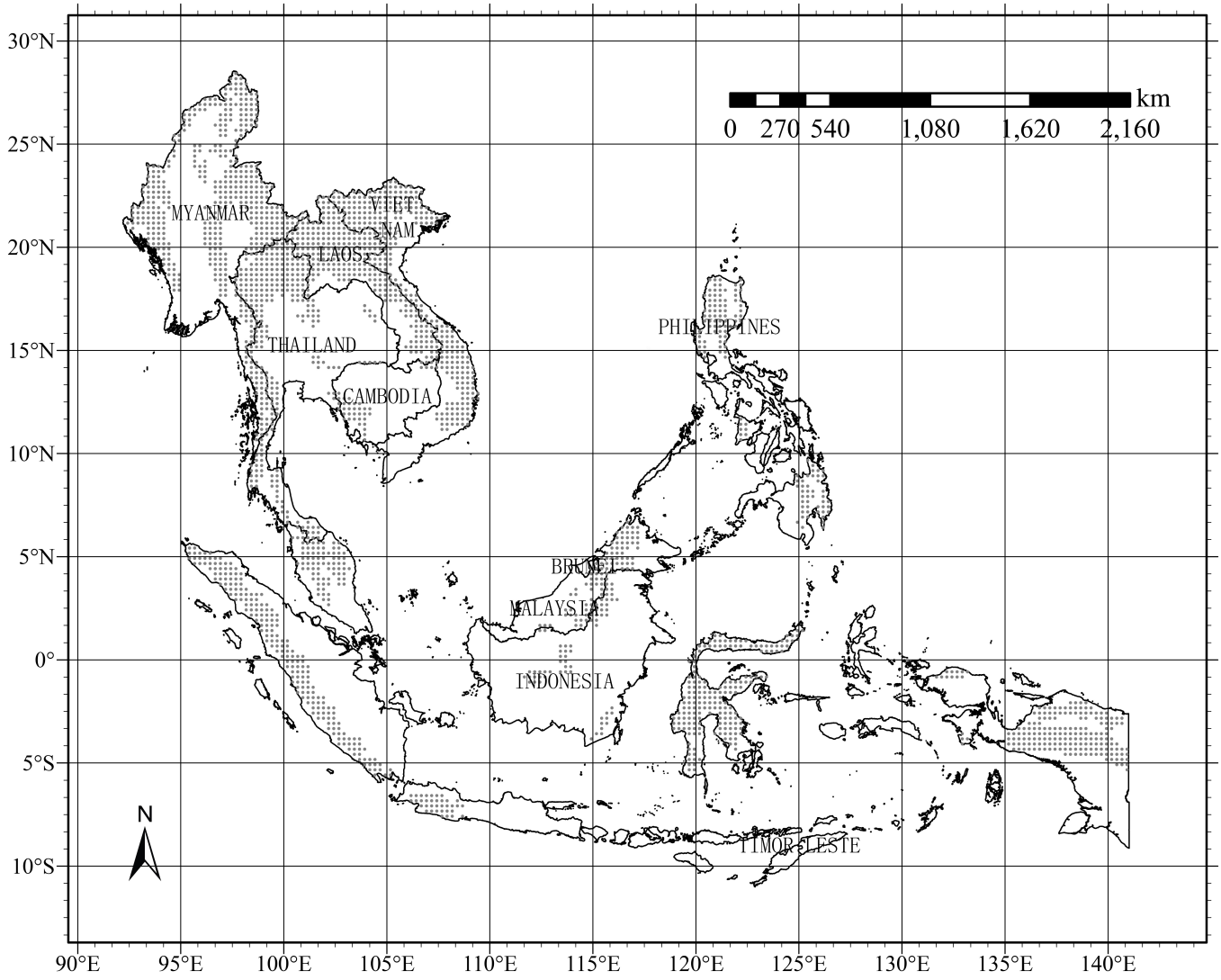

Fig. 1. Geographical location of the study area (black points represent highland regions with elevations above 300 m).

and −11.00° to 28.55°N. Based on the Global Mountain Biodiversity Assessment (GMBA), about 1.7 million km^2 (38%) of this area's land surface are mountains (black points in Fig. 1; [56]).

Agricultural expansion is currently a key driver of forest loss in SEA, where dramatic acceleration in forest loss was found in highlands (areas above 300-m elevation) over the last decade [11,57,58]. A recent study suggested that 7 of the SEA countries made the list of the world's top 15 in forest carbon loss during the 21st century, including Cambodia, Indonesia, Lao PDR, Malaysia, Myanmar, Thailand, and Vietnam [57]. In Indonesia and Malaysia, high forest loss was largely driven by the expansion of commodity agriculture, including oil palm [11]. In other countries, forest loss was associated with both commodity and small-scale agriculture expansion [59]. The extent of forest loss and its complex drivers make SEA an ideal region for our analysis, which focuses on the uncertainties in forest loss mapping in complex terrain [57,60].

Satellite data

Planet's satellite imagery

We used Planet optical imagery (https://www.planet.com/nicfi/) to label samples, train the classification algorithm, and map the classification results. Planet operates the SkySat and PlanetScope Earth-imaging constellations, which contain 200 satellites. SkySat is a constellation of 21 high-resolution Earth-imaging satellites that have been launched gradually since 2013 ([50]; https://www.planet.com/products/). The SkySat constellation has a sub-daily revisit time, collecting images over the same target area up to 6 to 7 times, with a maximum of 12 times per day. Individual satellites have a 4- to 5-day revisit time on average, and they are capable of capturing up to 400 km^2 day^{-1}. PlanetScope is a constellation of approximately 130 satellites that can image the entire Earth's surface each day (collection capacity of 200 million km^2/day). The constellations have a spatial resolution of 0.72 to 0.8 m for SkySat and 3.7 m for PlanetScope. Each satellite provides blue, green, red, and near-infrared (NIR) images.

Planet provides a basic scene product, an ortho scene product, and an ortho tile product, based on satellite product processing levels [50]. Importantly, Planet has reprocessed the SkySat and PlanetScope imageries through NICFI (https://www.planet.com/nicfi/) at the Ortho Tile product level, which selects the best imagery to represent every part of the coverage area during leaf-on periods from June to November based on cloud

cover and acutance (image sharpness). Non-commercial users can freely access the 4.77-m semiannual analysis-ready mosaics of the world's tropics for the years 2015 to 2022 [52]. As the resolution varies with latitude, 4.77 m is the maximum pixel dimension, occurring at the equator. Moreover, the NICFI base maps incorporate advanced atmospheric correction and cloud masking algorithms, enhancing the quality of the imagery.

Sentinel-1 SAR imagery

Based on prior work demonstrating the applicability of SAR products for land-cover mapping [15,16,20], we chose the 10-m resolution dual-polarization Ground Range Detected (GRD) scene (VV + VH) aboard Sentinel-1 to map tropical forests from 1 June 2019 to 30 November 2019 in the GEE platform. We selected the SAR data to address potential overestimation resulting from confusion with herbaceous vegetation, as well as potential underestimation due to optical satellite observations omitting deciduous or semi-deciduous characteristics [16]. Briefly, the Sentinel-1 satellites acquire C-band SAR imagery independent of time of day or weather [53]. Sentinel-1 A and B were launched in April 2014 and April 2016, respectively. Their repeat cycle is 12 days for a single satellite or 6 days for a dual-satellite constellation. Sentinel-1 SAR data products provide single polarization (VV or HH) for Wave mode, and dual (VV + VH or HH + HV) or single (HH or VV) polarization for SM, IW, and EW modes. The GEE platform contains all of the GRD scene data from October 2014 to the present [52]. Each scene has one of 3 resolutions (10, 25, or 40 m), 4 band combinations (VV, HH, VV + VH, and HH + HV), and 3 instrument modes (SM, IW, and EW). These data were pre-processed with the Sentinel-1 Toolbox for thermal noise removal, radiometric calibration, and terrain correction.

Mapping approach

To undertake our assessment, and to improve fine-scale mapping of forest cover, we developed a machine-learning approach that applied the Random Forests (RF) model [61] to Planet and Sentinel-1 imagery within the GEE platform. The workflow involved collecting satellite imagery and existing land cover products, constructing labeled samples, developing an RF classifier, and implementing the machine learning algorithms into

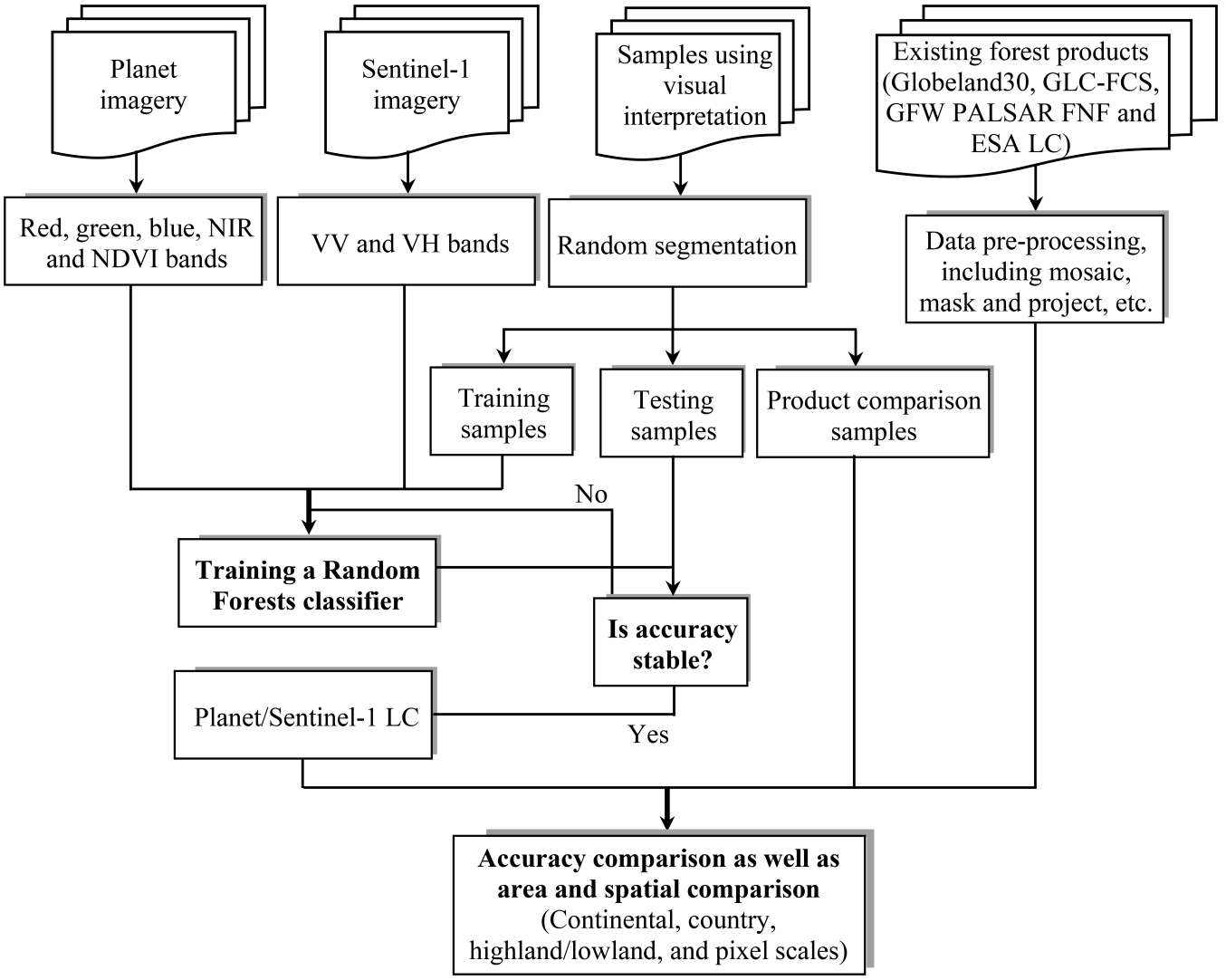

Fig. 2. Workflow for mapping Planet/Sentinel-1 LC and area as well as spatial comparisons among existing high-resolution forest cover products.

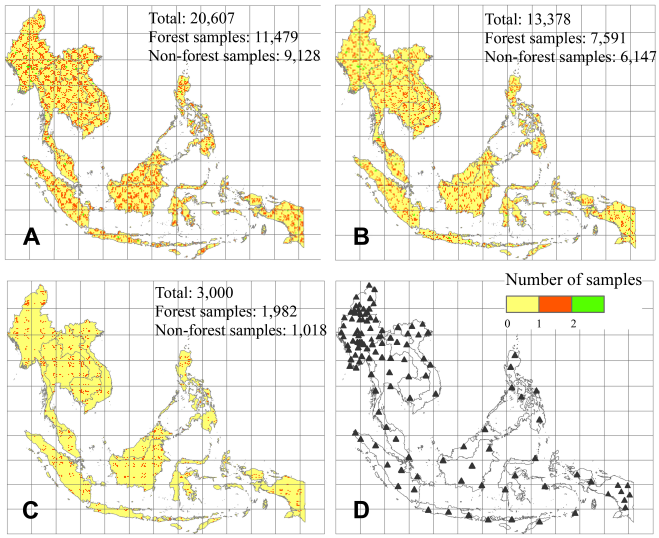

Fig. 3. Spatial distributions of labeled samples using visual interpretation and randomly selected Planet scenes of each 2 × 2° grid cell. (A) Training samples, (B) testing samples, (C) product comparison samples, and (D) randomly selected scenes within each 2 × 2° grid cell. The number of samples is aggregated into 100 km^2.

Table 1. Inputs for mapping Planet/Sentinel-1 forest cover product.

Satellite band type	Spatial resolution/m	Temporal resolution	Function
Planet red band Planet green band Planet blue band Planet NIR band Planet NDVI band	4.77	Biannual (December to May and June to November)	Identify the 2-dimensional structure of vegetation and particularly foliage cover
Sentinel-1 VV band Sentinel-1 VH band	10	6-day/12-day repeat cycle	Relate to structure and biomass information of forests

which labeled samples were separated into training, testing, and product comparison datasets (Fig. 2). We defined trees as all vegetation over 5 m in height, labeled as forest pixels. To investigate the performance of the method, we compared the Planet/Sentinel-1 forest cover with existing forest cover products of various resolutions (i.e., Globeland30, GLC-FSW30, GFW LC, PALSAR FNF, and ESA LC) as well as selected FAO Forest Resource Assessments (see below).

Construction of labeled samples

A total of 37,345 samples (at ≤4.77-m resolution) were labeled forests and non-forests by visual interpretation of Planet imagery in 2019, including the following: 20,607 training samples (Fig. 3A; 11,479 forest samples and 9,128 non-forest samples), 13,738 testing samples (Fig. 3B; 7,591 forest samples and 6,147 non-forest samples), and 3,000 product comparison samples (Fig. 3C; 1,982 forest samples and 1,018 non-forest samples). We mapped samples without orchards and plantations.

During the labeling stage, 23,046 random points within the entire study area were first generated. The points were then manually identified in QGIS as forests and non-forests using online Planet base maps in the Planet's Explorer and the tree height of [62]. Another 14,499 samples were manually labeled in randomly selected Planet scenes of each 2 × 2° grid cell (Fig. 3D), based on locally downloaded Planet imagery at the polygon level, which was collected to ensure precise identification of land use types in some locations related to complex underlying surface environments, such as the deforestation frontiers and boundary changes related to a variety of contemporary activities.

Finally, 3,000 samples were randomly extracted from the labeled 23,046 samples to compare the mapped Planet/Sentinel-1 forest cover with existing forest cover products (Fig. 3C). The remaining samples were combined with the 14,499 samples (a total of 34,345 samples) to train and test the RF model.

Developing an RF classifier

Machine learning algorithms have already demonstrated their effectiveness in creating land-cover and land-use change (LCLUC) maps [9,63,64]. RF-based ≥machine learning algorithms in particular have been widely applied to mapping LCLUC [23,65] because of their relatively simple and accurate ensemble [61,66]. By applying a "wisdom of crowds" approach, the RF algorithm aggregates numerous, independently trained decision trees to learn from a diverse set of data, leading to stable and generalizable prediction results. Each tree in the RF makes a class prediction, and the class with the most votes becomes the model's prediction [61].

The first step in developing the RF-based machine learning algorithms involved preparing 7 inputs (Table 1) for mapping Planet/Sentinel-1 forest cover products, including the reflectance values from the Planet red, green, blue, and NIR bands, the normalized difference vegetation index (NDVI) calculated from the red and NIR bands, Sentinel-1 VV and VH values, and binary raster (forest/non-forest labels). After loading the second biannual Planet red, green, blue, and NIR bands (i.e., the time window is June to November) and the Sentinel-1 VV/VH bands from 1 June 2019 to 30 November 2019 in the Earth Engine Data Catalog, we leveraged the GEE mosaic function to produce spatially continuous SAR imagery and resampled it using bilinear interpolation to match the spatial resolution of Planet imagery. The NDVI band was calculated as follows [67]:

$$\mathrm{NDVI} = \frac{\mathrm{NIR} - \mathrm{red}}{\mathrm{NIR} + \mathrm{red}} \quad (1)$$

where red and NIR represent Planet red and NIR bands, respectively. The training (Fig. 3A) and testing (Fig. 3B) samples in the previous section were matched with the input imagery based on the same geolocations to obtain a set of predictors that were randomly segmented into training and testing datasets. Then, the RF model parameters were set to 100 trees with others remaining at their default values. Next, the RF models were trained and tested repeatedly until the accuracy stabilized (see the next section). The trained model was then used to

create predictions within 2 × 2° grid cells, which were used to reduce the amount of data per serving, followed by several post-processing steps (mosaic, mask, project, etc.), resulting in final classification maps for the SEA region that constitute the Planet/Sentinel-1 forest cover product for 2019.

To evaluate the degree to which Sentinel-1 added extra information that helped the classifier distinguish between forest and non-forest, we trained 2 versions of the model: one using only the Planet variables, and the other including both Planet and Sentinel-1 variables.

Accuracy assessment of the classification map

The performance of the RF classifiers was assessed using the 9,738 testing samples (Fig. 3B). The assessment was based on the F1 score [68], overall accuracy, producer accuracy, and user accuracy, which was based on the confusion matrix [69]. Here, we had not adopted confidence intervals for accuracy measures because of the supplemented polygon samples [49,70,71]. Additionally, the model training and testing were repeatedly performed to minimize the impacts of unevenly distributed trained and tested samples on the RF model.

Comparison with existing forest cover products

Finally, we compared our Planet/Sentinel-1 forest cover map with other forest cover products through the sample- and area-based assessments, as well as through spatial comparison at the cell level to investigate how well the rounding error was resolved within different geographies, such as within different countries or for montane areas [15,16]. The other forest cover products included the following (Table 2): (a) Globeland30 [17], (b) the global 30-m land-cover classifications with a fine classification system (GLC-FCS30; [21,22]), (c) Global Forest Watch (GFW)-LC [9], (d) European Space Agency land cover (ESA-LC; [20]), and (e) PALSAR forest/non-forest map (FNF; [16]). We also used country forest statistics data from the Forest Resources Assessment (FRA) of the Food and Agriculture Organization (FAO) to assess our classification map at the country scale [18]. To create forest cover maps from the 3 land cover datasets (1, 2, and 4), we converted all forest-related and non-forest classes into 2 separate classes to produce binary maps. It can be challenging to select images with the same time reference to reduce errors in our mapping process. However, we have made efforts to choose images that are as closely aligned as possible with the time of our mapping, to minimize any discrepancies.

In the sample-based evaluation stage, we compared the performance of our maps with that of existing forest cover products using the 3,000 product comparison samples (Fig. 3C) at ±95% confidence intervals [70].

To compare the variability in forest inventory estimates arising from each product, we calculated from each set of maps the total forest cover for each country in the SEA region, as well the total forested area in lowland and highland regions.

We also examined the degree of rounding error by aggregating our maps to the coarser resolution of existing forest cover products, then estimating forest cover areas to those calculated from the coarser products. Note that we had not used confidence intervals for area estimates, as these were estimated for different scales (the continent, countries, and highland/lowland areas). For simplicity, but consistent with past analyses, we defined highlands as areas with elevations above 300 m [11,56,72]. This topographic division primarily distinguishes mountainous areas from flatter terrain, but we recognized that not all lands above 300 m above sea level are mountains per se, and some mountainous areas occur at lower elevations.

Table 2. Descriptions of existing forest cover products used for comparison.

Forest cover product	Forest definition	Sensor	Spatial resolution (m)	Year	Source
Globeland30	Tree cover ⩾ 15%, tree height ⩾ 5 m	Landsat TM/ETM+/OLI	30	2020	http://www.globalland-cover.com/
GLC-FCS30	Tree cover ⩾ 15%, tree height ⩾ 5 m	Landsat TM/ETM+/OLI	30	2020	https://zenodo.org/record/4280923#.Yj40FdAzaUk
GFW	Tree cover ⩾ 15%, tree height ⩾ 5 m	Landsat TM/ETM+	30	2019	www.globalforestwatch.org
ESA LC	Tree cover ⩾ 15%, tree height ⩾ 3 m	Sentinel-1 SAR and Sentinel-2 MSI	10	2020	https://viewer.esa-worldcover.org/worldcover/
PALSAR FNF	Tree cover ⩾ 10%, tree height ⩾ 5 m	PALSAR	25	2017	https://developers.google.com/earth-engine/datasets/catalog
FAO FRA	Tree cover ⩾ 10%, tree height ⩾ 5 m	NA	Country scale	2019	https://www.fao.org/forest-resources-assessment/fra-2020/country-reports/
Planet/Sentinel-1 LC	Tree height ≥ 5 m	SkySat + PlanetScope and Sentinel-1	4.77 m	2019	This study

Results

Classification results

Based on the test samples (Fig. 3B), the overall accuracy, F1 score, producer's accuracy, and user's accuracy of our Planet/Sentinel-1-based forest map for 2019 were 0.937, 0.942, 0.953, and 0.931, respectively (Table 3). These scores are slightly higher than those for the Planet-only forest cover map for 2019, which were 0.908, 0.923, 0.942, and 0.905, respectively. The improvement associated with the incorporation of Planet and Sentinel-1 compared with using only the Planet optical imagery (Table 3) mainly results from the additional information on the structure and forest biomass provided by SAR imagery [16,25,73]. This confirmation was supported by comparing forest cover maps generated using imagery from both Planet and Planet/Sentinel-1 (Fig. S1), as well as by considering the importance calculated from the individual band input analysis, which revealed high importance values for VV and VH bands (Fig. S2). The producer's and user's accuracies for non-forest classifications also showed similar levels of improvement in the Planet/Sentinel-1 version compared to the Planet-only variant (Table 3).

As seen in Fig. 4, large areas of montane forests occur in Indonesia, Malaysia, and the highlands of mainland SEA, while only a small fraction of the lowlands were forested. The total forest area determined with the Planet/Sentinel-1 approach was approximately 3,236,276 km^2 (68.6%), with Indonesia having the largest forest area (1,571,977 km^2) and Brunei the smallest (5,383 km^2) (Fig. 4). We excluded Singapore from this analysis as the forested area is just ~160 km^2. Forests in montane SEA total 1,445,479 km^2, indicating that ~85% of the mountain area (1.7 million km^2) is forested. In addition, the mountain share of the region's total forested area (44.7%) exceeded the 38% estimated by Körner et al. [56] in a recent global mountain inventory.

We further assessed our classification results by comparing our Planet/Sentinel-1 map and ESA forest maps to Planet imagery (Figs. 5 to 7) at 6 locations that represent the variety of landscape complexities found in both the highlands and the lowlands (red points in Fig. 4). We found good visual agreement between our classification results and the original Planet imagery, distinguishing clearly between forested and non-forested areas that were associated with residential areas, roads,

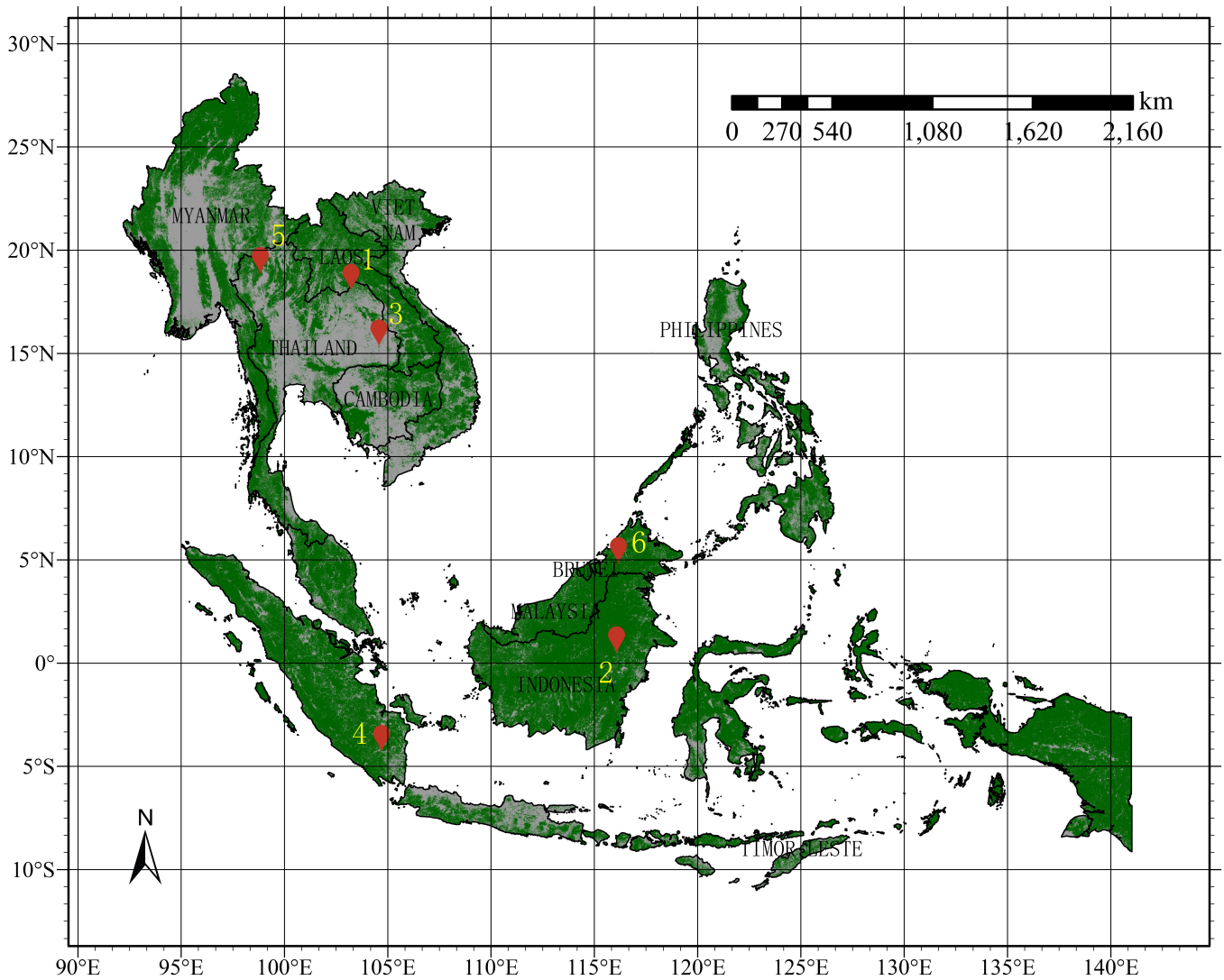

Fig. 4. Classification maps of forests (green) and non-forests (gray) using Planet and Sentinel-1 imageries in 2019. Red points represent the 6 selected areas of enlarged Planet imagery as well as Planet/Sentinel-1 and ESA forest maps (Figs. 5 to 7).

Table 3. Evaluation of Planet/Sentinel-1 forest maps.

Satellite sources	Land cover type	Overall accuracy	Producer's accuracy	User's accuracy	F1 score
Planet/ Sentinel-1	Forests	0.937	0.953	0.931	0.942
	Non-forests		0.918	0.943	
Planet only	Forests	0.908	0.942	0.905	0.923
	Non-forests		0.860	0.913	

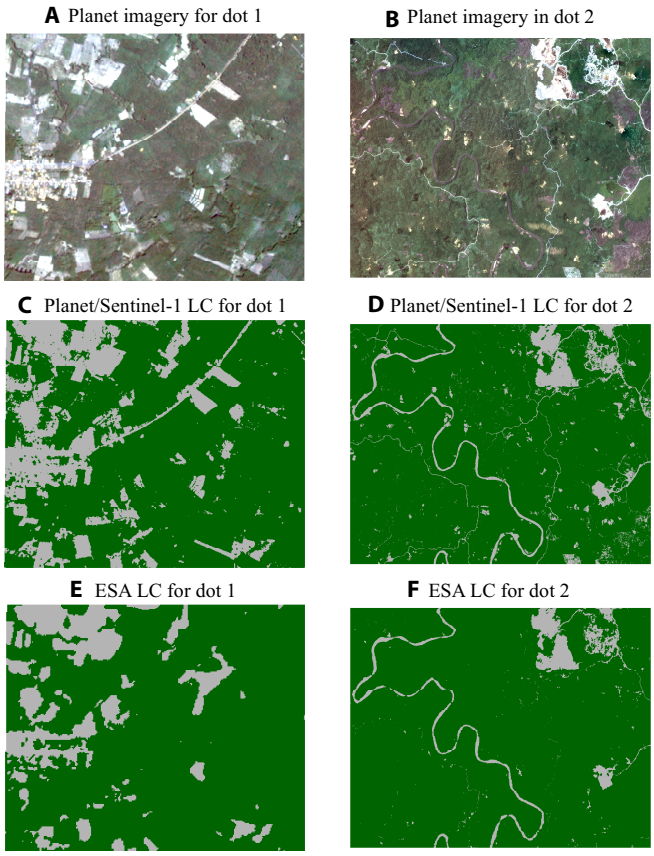

Fig. 5 Enlarged Planet imagery as well as Planet/Sentinel-1 and ESA forest maps for 2 selected focus locations for assessment of built-up fields in the lowlands. (A and B) Planet imageries, (C and D) Planet/Sentinel-1 forest map (this study), and (E and F) ESA forest maps for focus points 1 and 2 in Fig. 4.

highland deforestation, and other small-scale features. In comparison, the ESA LC classification was less consistent with the Planet imagery collected from a similar period, likely due to the coarser satellite imagery used in the ESA LC. Noticeable in the ESA LC map was the inability to capture small forest fragments and the greater irregularity of many forest edge boundaries (Figs. 5 to 7). The discrepancy between the 6 maps supports our underlying premise that high-resolution satellite imagery is crucial for mapping land cover accurately in complex and often fragmented environments. The forest area for the 6 map scenes ranges between 4.5 and 123.1 km^2 by Planet/Sentinel-1 LC (5-m resolution) versus 4.6 and 128.0 km^2 by ESA LC (10-m resolution) (Table 4), with a relative difference between the 2 LC products (ESA − Planet/Sentinel-1) ranging from −4.4% (Map scene 5) to +36.8% (Map scene 4). In general, the ESA product tended to overestimate forested areas relative to our maps. The comparison shows the ability of the high-resolution satellite approach to classifying small, isolated forest patches and large individual trees as well as small or narrow areas of non-forest.

Accuracy comparison of forest cover products

We also compared the performances of our new forest cover map with existing mainstream forest cover products at ≥25-m resolutions generated using optical-only, SAR-only, or both sensors. Specifically, a comparison of our Planet/Sentinel-1 forest map with 5 existing forest products (i.e., Globeland30, GLC-FCS30, GFW LC, PALSAR FNF, and ESA LC) at 3,000 randomly selected samples (Fig. 3C; ±95% confidence intervals) showed that the Planet/Sentinel-1 LC approach performed the best with an overall accuracy of 0.896 ± 0.011 (Table 5). The optical-only or SAR-only forest products with coarser resolution (≥25 m) exhibited lower accuracy than our mixed approach. The 10-m ESA LC map had higher producer's (0.915 ± 0.011) and overall (0.804 ± 0.014) accuracies than the other methods but with a lower user's accuracy of 0.811 ± 0.016. We observed that GLC-FSW30 and PALSAR exhibited lower user's accuracies, which can be attributed to the stringent filters applied to the training data for GLC-FSW30 and the limitation in identifying low-height bushes for PALSAR. Thus, the combination of SAR and optical Planet imagery can achieve higher accuracy in mapping forest cover than existing forest cover products with medium resolutions. However, one must understand that it is not completely fair to assess the accuracy of the other forest cover maps against a benchmark derived from labels developed specifically for this study.

Resolution of rounding errors

We investigated how well-rounding errors were resolved by our Planet-Sentinel 1 forest cover map by comparing total forest area estimates and differences in pixel-based estimates of fractional forest cover relative to other products. Again, rounding errors occur when one or more land-cover types constituting the minor share of a pixel are classed as the type covering the larger share.

Comparison of forested area estimates

We found large differences in national-scale forest cover estimates derived from the various products (Table 6). Notably, the FAO estimates are the lowest, likely because assessments are derived from reports by officially nominated national correspondents, and supplemented with remote sensing-based analysis [18]. The estimates for the other 6 products ranged from 2.616 million (PALSAR FNF) to 3.493 million km^2 (ESA LC). The country-specific forest cover estimates calculated from ESA LC were higher than our Planet/Sentinel-1 LC estimates for 9 of 11 SE Asian countries, ranging from 2% lower in Cambodia to 28% higher in Thailand (Table 6). Conversely, the PALSAR FNF forest cover estimates were lower in 9 of 11 countries than those determined using our approach, varying from −52%

(Philippines) to +8% (Myanmar). The closest estimates to ours were those based on Globeland30. The range in differences was −14% for Vietnam and +17% for Myanmar. The total forest area estimated by these 2 products was 3.236 and 3.188 million km^2 for Planet/Sentinel-1 LC and Globaland30, respectively. In general, estimates from the lower-resolution products tended to be lower than ours, except for ESA LC, which yields the highest forest cover amount (3.493 million km^2) despite having a resolution of only 10 m, likely because of the lower tree height definition. This departure suggests that, although fine-resolution forest products can detect more patches than those developed from coarser-resolution imagery [14,39,48], other aspects of the classification approaches to influence the outcome, such as choices made during the model development process.

Forest cover estimates derived from the different products for lowland and highland areas in SEA showed similar patterns to the country-level comparisons (Table 7). The ESA LC-based estimates were 8% higher than those of Planet/Sentinel-1 LC for both lowlands and highlands, while Globeland30 again produced values similar to those of Planet/Sentinel-1 LC, with an estimate that was 3% higher for lowlands and 5% lower for highlands. The other products had cover estimates that ranged between 2 and 29% lower for lowlands and highlands relative to Planet/Sentinel-1 LC. For all products, the classification differences, relative to our product, were highest for the lowlands, which is a result that is contrary to our premise that resolution differences among products would manifest the most in montane areas [11,14,57]. For example, the lowland forest cover estimate from the Globaland30 product was 90 million km^2 lower than from Planet/Sentinel-1, while the highland estimate was 42 million km^2 higher. Furthermore, the more than 257 million km^2 difference in the forest cover estimate from ESA LC relative to ours is primarily related to forest differences in the lowland area (+140 million km^2), rather than the highlands (+117 million km^2). This result reflects a higher degree of fine-scale complexity in lowland landscapes, such as solitary trees, rock outcrops, and linear road and stream features, that cannot be easily resolved with coarse-scale sensors.

Comparison of pixel-scale fractional cover estimates

We aggregated the pixels in our product from the original 4.77-m spatial resolution to match the resolutions (10, 25, and 30 m) of the 5 corresponding forest cover products, converting the classifications into fractional cover estimates within those cells having forest cover in the other product. Figure 8A shows the spatial distribution of forest cover fractions aggregated into the Globeland30 map, while the fractional cover maps based on the other products are shown in Figs. S3 to S6. Although there were differences in forest cover locations between the different products, we found that pixels with lower forest cover fractions are consistently located along known deforestation frontiers (Fig. 8A). Forest fractions in the Greater Mekong Subregion also tended to be smaller than those in maritime SEA, with values typically less than 0.6. The geometrically irregular forms along deforestation frontiers, therefore, tend to cause large uncertainties in existing forest cover products, even though the resolution of the satellite imagery used to make them is relatively high (25 to 30 m). The map aggregated to ESA LC forest pixels had larger fractional cover values than

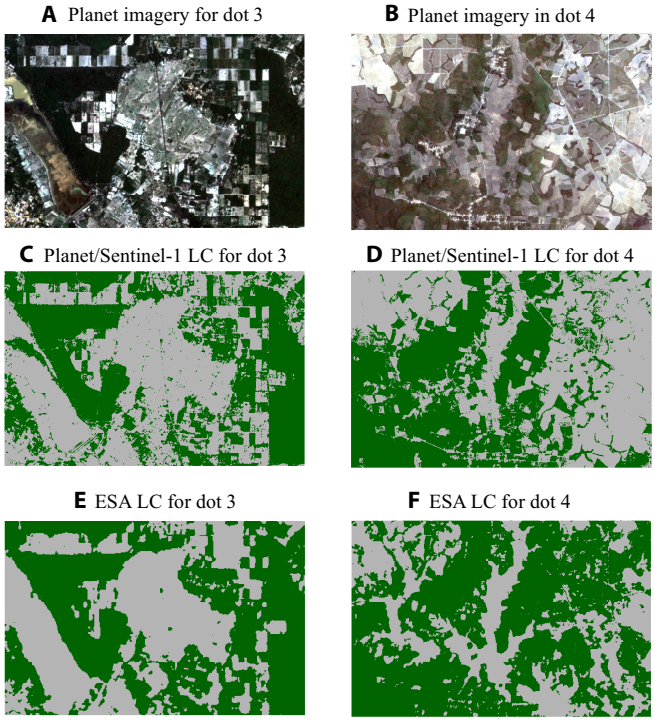

Fig. 6. (A to F) Same as Fig. 5, but for assessment of dominant croplands in the lowlands.

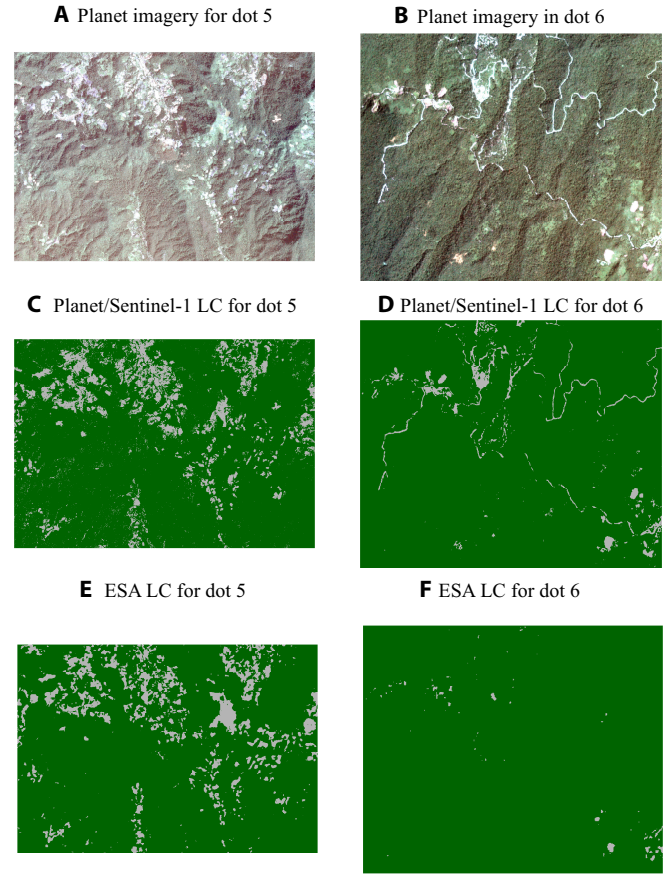

Fig. 7. (A to F) Same as Fig. 5, but for assessment of forest extent in the highlands with elevations above 300 m.

those created to match other forest cover products at the same locations (Fig. 8), given the lower omission error in that product, which further verifies that higher-resolution imagery improves forest cover estimates.

We further calculated the proportions of forest cover fraction maps, as depicted in Fig. 8 and Figs. S3 to S6, within specific intervals: 0 to 0.1, 0.1 to 0.25, 0.25 to 0.4, 0.4 to 0.6, 0.6 to 0.8, and 0.8 to 1. We chose the intervals of 0 to 0.1 and 0.1 to 0.25, which are commonly used thresholds for defining forests by FAO [18] and Hansen et al. [74]. The proportion results are shown in Fig. 9 and Table S1. Our findings revealed that the forest cover maps within the intervals of 0 to 0.8 all exhibited non-negligible proportions ranging from 0.011 to 0.036 (Fig. 9 and Table S1). Meanwhile, the forest cover maps within the intervals of 0 to 0.1 and 0.1 to 0.25 showed proportion ranges of 0.011 to 0.016 and 0.014 to 0.022, respectively. This indicates that using coarser satellite imagery may result in an underestimation of forest cover areas. For instance, in the case of Globeland30 forest cover fraction maps, the underestimated areas within the intervals of 0 to 0.1 and 0.1 to 0.25 were 47,831 km^2 and 63,457 km^2, respectively.

Discussion

High-resolution mapping of forest cover

The mixed method for mapping forest cover that we developed provides the most detailed and accurate forest cover product developed to date for SEA, improving on classification accuracy results because high-resolution Planet imagery helps reduce the magnitude of rounding errors when classifying forest cover ([35,37,41]; Fig.8A and Figs. S1 to S4). Improvements were most evident in complex lowland areas and along deforestation frontiers, where numerous isolated trees and small or narrow forest clearings are more numerous, which are features that the Planet/S1 approach identified more precisely than the higher-resolution (10-m) ESA LC product (Figs. 5 to 8).

Rounding errors occur at any scale of classification of a remote sensing product [14,15,37,75–77]. Some early studies addressed the impacts of "boundary effect" and "within-class variability" on rounding errors based on multisource data, such as on-field data, airborne data, or a scene simulation [35,37,41]. Recently, several researchers drew attention to this issue along deforestation frontiers, locations with small-scale cultivated fields, areas with selective logging, and forest extent in dryland biomes [27,39,47,75]. These studies all verify that the inability to map very small patches and irregular boundaries accurately potentially adds uncertainty to initiatives to track forest loss and gain at coarse-to-medium resolutions.

The manifestation of rounding errors was evident in the forest cover products we derived from existing land cover maps, which had substantially different (typically smaller) estimates of the forested area than those based on our map. A substantial portion of these differences can be explained by the failure of coarser resolution products to accurately map large solitary trees and small or narrow forest clearings, which are inherently part of total tree cover, but not necessarily "forest." The exception to this pattern of differences was seen in the ESA-LC product, which generally produced larger forested area estimates than our product. In this case, the difference was mainly due to the product misclassifying non-forest as forest, particularly smaller patches; thus, rounding errors were more linked to non-forest cover.

These findings related to rounding errors are in line with earlier work demonstrating how classification error associated

Table 4. Area comparisons of the mapping new forest cover and ESA LC at 6 locations.

Map scene	Elevation/m	Area/ km^2	Total forest area/ km^2	Area difference (%)	
			Planet/ Sentinel-1 LC	ESA LC	
1	182	5.8	4.5	4.6	0.1 (3.6)
2	68	136.1	123.1	128.0	4.9 (4.0)
3	127	11.5	5.4	5.9	0.5 (9.7)
4	36	19.1	9.0	12.4	3.4 (36.8)
5	1,050	53.7	47.4	45.3	−2.1 (−4.4)
6	845	20.0	19.3	19.9	0.6 (3.0)

Note: Area difference indicates ESA LC minus Planet/Sentinel-1 LC, and the values in parenthesis express the area difference as a percentage relative to the area of our forest product.

Table 5. Accuracy comparison of different forest cover products at ±95% confidence intervals (based on 3,000 random samples).

Sensor	Forest product	User's accuracy	Producer's accuracy	Overall accuracy
Optical	Globeland30	0.816 ± 0.017	0.837 ± 0.013	0.768 ± 0.015
	GLC-FSW30	0.891 ± 0.015	0.751 ± 0.013	0.774 ± 0.014
	GFW LC	0.858 ± 0.016	0.808 ± 0.012	0.781 ± 0.014
SAR	PALSAR	0.858 ± 0.017	0.719 ± 0.013	0.735 ± 0.015
Optical/ SAR	ESA LC	0.811 ± 0.016	0.915 ± 0.011	0.804 ± 0.014
	Planet/ Sentinel-1 LC (this study)	0.911 ± 0.011	0.931 ± 0.011	0.896 ± 0.011

Table 6. Country-wide comparison (km^2) of different forest cover estimates by the products considered.

Country name	FAO FRA	Globeland 30	GLC-FCS30	GFW LC	PALSAR FNF	ESA LC	Planet/Sentinel-1 LC
Lao PDR	16,768	205,397	136,542	185,523	198,477	201,340	200,411
Timor Leste	9,225	9,299	10,086	8,965	7,953	10,059	8,801
Cambodia	82,241	94,765	81,138	86,390	70,529	89,679	91,131
Philippines	71,537	202,734	191,027	198,603	99,672	235,013	207,757
Thailand	199,090	230,362	178,905	221,755	236,721	300,066	233,851
Vietnam	145,672	171,125	117,227	172,649	153,421	231,939	199,759
Brunei	3,800	5,308	4,924	5,214	4,897	5,279	5,368
Myanmar	288,336	506,330	439,733	486,800	469,714	508,692	434,146
Malaysia	191,642	279,977	212,807	218,544	217,967	300,777	283,297
Indonesia	927,387	1,483,353	1,268,690	1,401,234	1,157,244	1,610,917	1,571,857
Total	2,085,230	3,188,652	2,641,080	2,985,678	2,616,596	3,493,761	3,236,378

with pure pixels tends to increase due to within-class variability [35,37,41]. The use of very high-resolution imagery tends to improve the classification of the smallest phenomenon. What was less expected from our results was that the improvements caused by minimizing rounding errors appeared to have a larger impact, as measured by differences in forested area estimates, in the lowlands than in the highlands. Previous work suggested that moderate-resolution land cover products have more error in the highlands than in the lowlands [11]; therefore, we expected larger forested area differences there (Table 7). However, the lowlands have already experienced extensive deforestation and contain a broad mix of land uses [78], particularly agriculture, creating a complex terrain that includes many small isolated trees and forest patches that presumably sum to a substantial area. In contrast, highland forests are still more intact and the major driver of forest loss has been relatively small agricultural clearings on hill slopes [11]; thus, beyond small clearings, the number of isolated forest tree patches that share the total area in the highlands is likely smaller than in the lowlands, resulting in smaller discrepancies in area estimates in the highlands.

Our modeling approach allowed us to investigate the degree to which high-resolution optical imagery from the recently available Planet constellation improves large-area forest cover mapping, individually and in combination with complementary remote sensing products, in this case, SAR. We found here that using Planet imagery on its own produced accurate (90.8%) forest cover maps (Table 3). In addition to improving the ability to detect isolated trees and forest patches, it greatly improves the delineation of narrow linear features inside forests that would normally be classified as trees due to rounding error in moderate-resolution products: e.g., roads and riparian systems (e.g., Figs. 5 and 8). This capability is valuable for identifying both legal logging road networks for forest management as well as the unregulated construction of roads/trails that support illegal logging [79]. However, despite these high accuracies, the model was noticeably improved by including Sentinel-1 SAR imagery (93.7%), despite its lower resolution, which came from notable increases in the producer's accuracy for the non-forest class and both the user's accuracy for both classes. Adding SAR provided extra information that further improved the ability to discriminate between forest and non-forest cover. Given its sensitivity to the third dimension of vegetation structure [16], whereas optical sensors primarily respond to 2-dimensional structure (particularly foliage cover), SAR helps to separate the forest from shorter vegetation cover types that may be less distinguishable in the optical wavelengths. This is particularly true of non-forest, dense vegetation types during leaf-on periods (e.g., shrublands), which may resemble forests in optical imagery [48,80,81]. Beyond this additional information, the combination of the 2 sensor types avoids data loss when the output of one of the sensors is compromised, for example, by

Table 7. Area statistics (km^2) of different forest cover products for mountains and lowlands in SEA.

Land type	Globeland 30	GLC-FCS 30	GFW LC	PALSAR FNF	ESA LC	Planet/Sentinel-1 LC
Mountains	1,488,035	1,287,271	1,419,734	1,346,113	1,562,537	1,445,579
Lowlands	1,700,616	1,353,809	1,565,945	1,270,483	1,931,224	1,790,799
Total	3,188,652	2,641,080	2,985,678	2,616,596	3,493,761	3,236,378
Mountains/total	0.4667	0.4874	0.4755	0.5145	0.4472	0.4467

cloud contamination in the case of optical sensors, or by layover and foreshortening effects that impact SAR in rugged terrain [28,82,83].

These findings build on recent work examining the effectiveness of fine-to-medium with multi-sensor mapping [15,16,48]. For example, Qin et al. [15], in comparing user accuracy and producer accuracy of forest products at 30- to 500-m resolutions, showed that maps made using optical-only data had the highest producer accuracies, while SAR-only or mixed sensors had higher user accuracies. Our results stand somewhat in contrast to this, as including SAR boosted producer's accuracy on average more than user's accuracy, although the user's accuracy improvements resulting from SAR were more uniform across both classes (~2.5 to 3 percentage points).

Uncertainties and future work in forest cover mapping

Despite these improvements to forest cover mapping, uncertainties and errors remain to be addressed. For example, the approach erroneously classified some gaps in intact forest

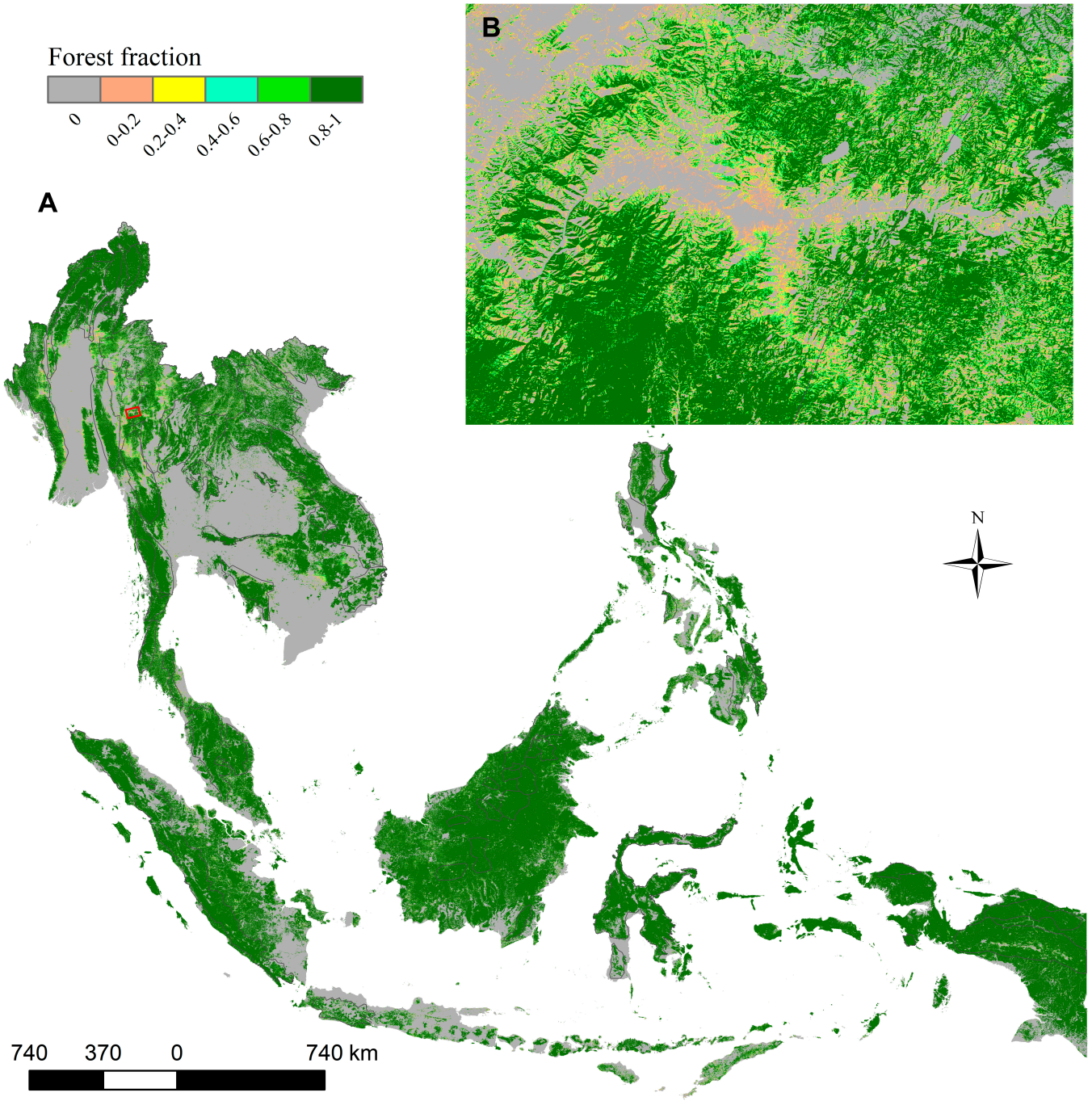

Fig. 8. Spatial distribution of forest cover fraction maps from Globeland30 in the SEA area. (A) The mapped 4.77-m Planet/Sentinel-1 LC product was aggregated into cells of Globeland30 and represented as the forest fraction (percentage) of the cell. (B) Zoom-in for the selected location of (A).

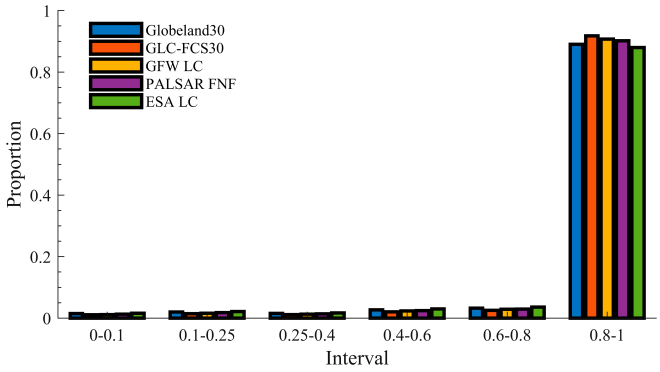

Fig. 9. The proportion of forest cover for each map within the interval of 0 to 0.1, 0.1 to 0.25, 0.25 to 0.4, 0.4 to 0.6, 0.6 to 0.8, and 0.8 to 1.

stands (Fig. 4), such as in places where rocky or pale soil was visible through the sparse canopy, particularly in the dry season when the understory was dry [75,84,85]. This issue relates to the degradation of classification accuracy with increasingly finer image resolution because of within-class variability inhomogeneous land covers [35,41]. Overcoming this limitation may be achieved through additional training on sparse canopy forests [48,80,86] or by applying filters to reduce the pixel noise [87]. In locations where forest cover and structure vary greatly, such as ridgelines with thin soils and sparse canopies, the classification may be improved through the incorporation of terrain indices, such as slope, aspect, and elevation [88].

Another source of uncertainty is the fact that many orchards and plantations are often classified as forests if unique spatial patterns and phenology cannot be discerned [83]. Further, while Planet can acquire high-resolution optical imagery at frequent time intervals, the resulting cloud-free imagery may not, in some cases, represent the maximum leaf-on period, which is often in the rainy season. Data from the maximum leaf-on period are critical for mapping forest extent accurately [23,43–45,89]. Beyond this, while SAR imagery can reduce classification errors that are common in optical-only forest cover maps, distinguishing unvegetated land cover types, such as buildings, rocky ground, and partially bare land, is complicated when their structural characteristics resemble forests [15]. Combining SAR and optical products helps resolve this issue. A final lingering issue is whether accuracy will be similar for mapping non-tropical forests with greater differences in seasonality.

Furthermore, it is challenging to distinguish between rounding errors and salt and pepper noise in the extracted forest cover data. Therefore, in the future, it is imperative to leverage deep learning algorithms for accurate forest cover extraction, as they have shown exceptional performance when applied to high-resolution optical satellite imagery. Additionally, the accuracy of our model may have been overestimated due to the use of homologous labeled samples for training and testing. Therefore, it is necessary to consider alternative methods for sample collection to train our developed model, such as automatic sample generation techniques [90].

Conclusions

In this study, we developed an improved fine-scale method using an RF model to map high-resolution tropical forest extent by integrating Planet and Sentinel-1 imagery in the GEE platform. We found that our classification maps achieved good performance for forest cover mapping in the SEA region and the overall accuracy and the F1 score of the Planet/Sentinel-1 forest map were 0.937 and 0.942, respectively. These gains came primarily from the ability of high-resolution Planet imagery to delineate fine-scale landscape objects, with further improvements provided by SAR's ability to separate the forest from optically similar non-forest cover types. This high-resolution multi-sensor approach produced maps that were more accurate than those derived from existing products based on moderate-resolution imagery. The accuracy and finer-grain of our approach help to resolve the rounding errors that arise in moderate-resolution imagery, when small features are combined with a more prevalent class, as demonstrated in our comparison of forest cover estimates generated from our map with those derived from 10- to 30-m land cover maps (i.e., Globeland30, GLC-FSW30, GFW LC, and PALSAR FNF). By reducing such rounding errors, our maps generally produce larger estimates of lowland forest cover for the SEA region. However, despite the fact that our method showed a substantially improved ability to map forests accurately, our method and current products all have closer forest area estimates in the highlands than in the lowlands, likely because the small-scale phenomena that were more effectively detected using our approach—small forest patches (including large solitary trees) and small or narrow forest clearings—are more prevalent ubiquitous in highly heterogeneous lowland landscapes. We conclude that this improved fine-scale mapping approach has great potential to accurately monitor changes in forest cover dynamics over large regions, especially in regions where deforestation frontiers produce complex, fine-scaled inter-grading of forest and non-forest cover types. This approach also offers the potential for large-area mapping of other cover types characterized by isolated or patchy tree cover, such as savannas [91].

Acknowledgments

Funding: This study was supported by the National Natural Science Foundation of China (grant no. 42071022), the start-up fund provided by the Southern University of Science and Technology (grant no. 29/Y01296122), and the China Postdoctoral Science Foundation (grant no. 2022M711472). J.W. was supported by the Hung Ying Physical Science Research Fund 2021-22 and the Innovation and Technology Fund (funding support to State Key Laboratories in Hong Kong of Agrobiotechnology) of the HKSAR, China. **Author contributions:** Z.Z. designed the research; F.Y. performed the analysis and wrote the draft; L.D.E. contributed to the development of the map and model assessment methods. All authors contributed to the interpretation of the results and the writing of the paper. **Competing interests:** The authors declare that they have no competing interests.

Data Availability

Forest area statistics of FAO FRA at the country scale were collected from https://www.fao.org/forest-resources-assessment/fra-2020/country-reports/. Planet imagery, Sentinel-1 SAR imagery, and PALSAR FNF forest cover product are available on the GEE platform: https://developers.google.com/earth-engine/datasets/catalog/projects_planet-nicfi_assets_basemaps_asia, https://developers.google.com/earth-engine/datasets/catalog/

COPERNICUS_S1_GRD, and https://developers.google.com/earth-engine/datasets/catalog/JAXA_ALOS_PALSAR_YEARLY_FNF. Additionally, Planet imagery is collected from Planet's Explorer with QGIS. The other forest cover products (i.e., Globeland30, GLC-FCS30, GFW-LC, and ESA-LC) are collected from http://www.globallandcover.com/, https://zenodo.org/record/4280923#.Yj40FdAzaUk, and https://viewer.esa-worldcover.org/worldcover/, respectively. All datasets are also obtained on reasonable request from Z.Z. Code availability: The scripts used to generate all the results are in JavaScript (https://code.earthengine.google.com/?scriptPath=users%2Fyftaurus%2Fcodes%3APlanet_RF-LC_rac). Analysis scripts are also available on request from Z.Z.

Supplementary Materials

Figs. S1 to S6
Table S1

References

1. Brandon K. Ecosystem services from tropical forests: Review of current science. *Cent Glob Dev Work Pap.* 2014;38.
2. Martin TG, Watson JE. Intact ecosystems provide best defence against climate change. *Nat Clim Chang*. 2016;6(2):122–124.
3. Mitchard ETA. The tropical forest carbon cycle and climate change. *Nature*. 2018;559:527–534.
4. Raven PH, Gereau RE, Phillipson PB, Chatelain C, Jenkins CN, Ulloa Ulloa C. The distribution of biodiversity richness in the tropics. *Sci Adv*. 2020;6(37):eabc6228.
5. Richards DR, Thompson BS, Wijedasa L. Quantifying net loss of global mangrove carbon stocks from 20 years of land cover change. *Nat Commun*. 2020;11(1):1–7.
6. Roberts P, Hamilton R, Piperno DR. Tropical forests as key sites of the "Anthropocene": Past and present perspectives. *Proc Natl Acad Sci U S A*. 2021;118(40):e2109243118.
7. Saatchi SS, Harris NL, Brown S, Lefsky M, Mitchard ET, Salas W, Zutta BR, Buermann W, Lewis SL, Hagen S, et al. Benchmark map of forest carbon stocks in tropical regions across three continents. *Proc Natl Acad Sci U S A*. 2011;108(24):9899–9904.
8. Gillespie TW. Policy, drought and fire sear Amazon biodiversity. *Nature*. 2021;597(7877):481–483.
9. Hansen MC, Potapov PV, Moore R, Hancher M, Turubanova SA, Tyukavina A, Thau D, Stehman SV, Goetz SJ, Loveland TR, et al. High-resolution global maps of 21st-century forest cover change. *Science*. 2013;342(6160):850–853.
10. Pan Y, Birdsey RA, Fang J, Houghton R, Kauppi PE, Kurz WA, Phillips OL, Shvidenko A, Lewis SL, Canadell JG, et al. A large and persistent carbon sink in the world's forests. *Science*. 2011;333(6045):988–993.
11. Zeng Z, Estes L, Ziegler AD, Chen A, Searchinger T, Hua F, Guan K, Jintrawet A, Wood F. Highland cropland expansion and forest loss in Southeast Asia in the twenty-first century. *Nat Geosci*. 2018;11:556–562.
12. Zhao Z, Li W, Ciais P, Santoro M, Cartus O, Peng S, Yin Y, Yue C, Yang H, Yu L, et al. Fire enhances forest degradation within forest edge zones in Africa. *Nat Geosci*. 2021;14:479–483.
13. Achard F, Beuchle R, Mayaux P, Stibig HJ, Bodart C, Brink A, Carboni S, Desclée B, Donnay F, Eva HD, et al. Determination of tropical deforestation rates and related carbon losses from 1990 to 2010. *Glob Chang Biol*. 2014;20(8):2540–2554.
14. Chen H, Zeng Z, Wu J, Peng L, Lakshmi V, Yang H, Liu J. Large uncertainty on forest area change in the early 21st century among widely used global land cover datasets. *Remote Sens*. 2020;12(21):3502.
15. Qin Y, Xiao X, Dong J, Zhou Y, Wang J, Doughty RB, Chen Y, Zou Z, Moore B III. Annual dynamics of forest areas in South America during 2007–2010 at 50-m spatial resolution. *Remote Sens Environ*. 2017;201:73–87.
16. Shimada M, Itoh T, Motooka T, Watanabe M, Shiraishi T, Thapa R, Lucas R. New global forest/non-forest maps from ALOS PALSAR data (2007–2010). *Remote Sens Environ*. 2014;155:13–31.
17. Chen J, Chen J, Liao A, Cao X, Chen L, Chen X, He C, Han G, Peng S, Lu M, et al. Global land cover mapping at 30 m resolution: A POK-based operational approach. *ISPRS J Photogramm Remote Sens*. 2015;103:7–27.
18. FAO, *Global forest resources assessment 2020: Main report*. Rome: FAO; 2020.
19. Gong P, Wang J, Yu L, Zhao Y, Zhao Y, Liang L, Niu Z, Huang X, Fu H, Liu S, et al. Finer resolution observation and monitoring of global land cover: First mapping results with Landsat TM and ETM+ data. *Int J Remote Sens*. 2013;34(7):2607–2654.
20. Zanaga D, Van De Kerchove R, De Keersmaecker W, Souverijns N, Brockmann C, Quast R, Wevers J, Grosu A, Paccini A, Vergnaud S, et al. ESA WorldCover 10 m 2020 v100; 2021.
21. Zhang X, Liu L, Wu C, Chen X, Gao Y, Xie S, Zhang B. Development of a global 30 m impervious surface map using multisource and multitemporal remote sensing datasets with the Google earth engine platform. *Earth Syst Sci Data*. 2020;12:1625–1648.
22. Zhang X, Liu L, Chen X, Gao Y, Xie S, Mi J. GLC_FCS30: Global land-cover product with fine classification system at 30 m using time-series Landsat imagery. *Earth Syst Sci Data*. 2021;13(3):2753–2776.
23. Wang Y, Ziv G, Adami M, Mitchard E, Batterman SA, Buermann W, Marimon BS, Junior BHM, Reis SM, Rodrigues D, et al. Mapping tropical disturbed forests using multi-decadal 30 m optical satellite imagery. *Remote Sens Environ*. 2019;221:474–488.
24. Xu Y, Yu L, Ciais P, Li W, Santoro M, Yang H, Gong P. Recent expansion of oil palm plantations into carbon-rich forests. *Nat Sustain*. 2022;5:574–577.
25. Fan L, Wigneron JP, Ciais P, Chave J, Brandt M, Fensholt R, Saatchi SS, Bastos A, Al-Yaari A, Hufkens K, et al. Satellite-observed pantropical carbon dynamics. *Nat Plants*. 2019;5(9):944–951.
26. Li G, Lu D, Moran E, Dutra L, Batistella M. A comparative analysis of ALOS PALSAR L-band and RADARSAT-2 C-band data for land-cover classification in a tropical moist region. *ISPRS J Photogramm Remote Sens*. 2012;70:26–38.
27. Andersen HE, Reutebuch SE, McGaughey RJ, d'Oliveira MV, Keller M. Monitoring selective logging in western Amazonia with repeat lidar flights. *Remote Sens Environ*. 2014;151:157–165.
28. Reiche J, Lucas R, Mitchell AL, Verbesselt J, Hoekman DH, Haarpaintner J, Kellndorfer JM, Rosenqvist A, Lehmann EA, Woodcock CE, et al. Combining satellite data for better tropical forest monitoring. *Nat Clim Chang*. 2016;6(2):120–122.
29. Song XP, Hansen MC, Stehman SV, Potapov PV, Tyukavina A, Vermote EF, Townshend JR. Global land change from 1982 to 2016. *Nature*. 2018;560(7720):639–643.

30. Zhu Z, Evans DL. US forest types and predicted percent forest cover from AVHRR data. *Photogramm Eng Remote Sens*. 1994;60:525–531.
31. Baccini A, Walker W, Carvalho L, Farina M, Sulla-Menashe D, Houghton RA. Tropical forests are a net carbon source based on aboveground measurements of gain and loss. *Science*. 2017;358(6360):230–234.
32. Qin Y, Xiao X, Dong J, Zhou Y, Zhu Z, Zhang G, Du G, Jin C, Kou W, Wang J, et al. Mapping paddy rice planting area in cold temperate climate region through analysis of time series Landsat 8 (OLI), Landsat 7 (ETM+) and MODIS imagery. *ISPRS J Photogramm Remote Sens*. 2015;105:220–233.
33. Gong P, Liu H, Zhang M, Li C, Wang J, Huang H, Clinton N, Ji L, Li W, Bai Y, et al. Stable classification with limited sample: Transferring a 30-m resolution sample set collected in 2015 to mapping 10-m resolution global land cover in 2017. *Sci Bull*. 2019;64:370–373.
34. Karra K, Kontgis C, Statman-Weil Z, Mazzariello JC, Mathis M, Brumby SP. Global land use/land cover with Sentinel 2 and deep learning. Paper presented at: 2021 IEEE International Geoscience and Remote Sensing Symposium IGARSS: IEEE; 2021 July 11–16; Brussels, Belgium.
35. Hsieh PF, Lee LC, Chen NY. Effect of spatial resolution on classification errors of pure and mixed pixels in remote sensing. *IEEE Trans Geosci Remote Sens*. 2001;39(12):2657–2663.
36. Sexton JO, Noojipady P, Song XP, Feng M, Song DX, Kim DH, Anand A, Huang C, Channan S, Pimm SL, et al. Conservation policy and the measurement of forests. *Nat Clim Chang*. 2016;6(2):192–196.
37. Cushnie JL. The interactive effect of spatial resolution and degree of internal variability within land-cover types on classification accuracies. *Int J Remote Sens*. 1987;8(1):15–29.
38. Lu J, Huang C, Tao X, Gong W, Schleeweis K. Annual forest disturbance intensity mapped using Landsat time series and field inventory data for the conterminous United States (1986–2015). *Remote Sens Environ*. 2022;275:113003.
39. Matricardi EAT, Skole DL, Costa OB, Pedlowski MA, Samek JH, Miguel EP. Long-term forest degradation surpasses deforestation in the Brazilian Amazon. *Science*. 2020;369(6509):1378–1382.
40. Sugimoto R, Kato S, Nakamura R, Tsutsumi C, Yamaguchi Y. Deforestation detection using scattering power decomposition and optimal averaging of volume scattering power in tropical rainforest regions. *Remote Sens Environ*. 2022;275:113018.
41. Treitz PM, Howarth PJ, Suffling RC, Smith P. Application of detailed ground information to vegetation mapping with high spatial resolution digital imagery. *Remote Sens Environ*. 1992;42(1):65–82.
42. Ramo R, Roteta E, Bistinas I, van Wees D, Bastarrika A, Chuvieco E, van der Werf GR. African burned area and fire carbon emissions are strongly impacted by small fires undetected by coarse resolution satellite data. *Proc Natl Acad Sci U S A*. 2021;118(9):e2011160118.
43. Potapov PV, Turubanova SA, Hansen MC, Adusei B, Broich M, Altstatt A, Mane L, Justice CO. Quantifying forest cover loss in Democratic Republic of the Congo, 2000–2010, with Landsat ETM+ data. *Remote Sens Environ*. 2012;122:106–116.
44. Qiu S, Zhu Z, He B. Fmask 4.0: Improved cloud and cloud shadow detection in Landsats 4–8 and Sentinel-2 imagery. *Remote Sens Environ*. 2019;231:111205.
45. Sannier C, McRoberts RE, Fichet LV, Makaga EMK. Using the regression estimator with Landsat data to estimate proportion forest cover and net proportion deforestation in Gabon. *Remote Sens Environ*. 2014;151:138–148.
46. Zhao C, Qin C-Z. 10-m-resolution mangrove maps of China derived from multi-source and multi-temporal satellite observations. *ISPRS J Photogramm Remote Sens*. 2020;169:389–405.
47. Tyukavina A, Hansen MC, Potapov P, Parker D, Okpa C, Stehman SV, Kommareddy I, Turubanova S. Congo Basin forest loss dominated by increasing smallholder clearing. *Sci Adv*. 2018;4:eaat2993.
48. Velasco RF, Lippe M, Tamayo F, Mfuni T, Sales-Come R, Mangabat C, Schneider T, Günter S. Towards accurate mapping of forest in tropical landscapes: A comparison of datasets on how forest transition matters. *Remote Sens Environ*. 2022;274:112997.
49. Estes LD, Ye S, Song L, Luo B, Eastman JR, Meng Z, Zhang Q, McRitchie D, Debats SR, Muhando J, et al. High resolution, annual maps of field boundaries for smallholder-dominated croplands at National Scales. *Front Artif Intell*. 2022;4:744863.
50. Marta S. *Planet imagery product specifications*. San Francisco (CA): Planet Labs; 2018.
51. Roy DP, Huang H, Houborg R, Martins VS. A global analysis of the temporal availability of PlanetScope high spatial resolution multi-spectral imagery. *Remote Sens Environ*. 2021;264:112586.
52. Gorelick N, Hancher M, Dixon M, Ilyushchenko S, Thau D, Moore R. Google earth engine: Planetary-scale geospatial analysis for everyone. *Remote Sens Environ*. 2017;202:18–27.
53. Torres R, Snoeij P, Geudtner D, Bibby D, Davidson M, Attema E, Potin P, Rommen B, Floury N, Brown M, et al. GMES Sentinel-1 mission. *Remote Sens Environ*. 2012;120:9–24.
54. Azzari G, Jain S, Jeffries G, Kilic T, Murray S. Understanding the requirements for surveys to support satellite-based crop type mapping: Evidence from sub-Saharan Africa. *Remote Sen*. 2021;13(23):4749.
55. Rustowicz RM, Cheong R, Wang L, Ermon S, Burke M, Lobell D. Semantic segmentation of crop type in Africa: A novel dataset and analysis of deep learning methods. Paper presented at: Proceedings of the IEEE/CVF Conference on Computer Vision and Pattern Recognition (CVPR) Workshops; 2019.
56. Körner C, Jetz W, Paulsen J, Payne D, Rudmann-Maurer K, Spehn M, E. A global inventory of mountains for bio-geographical applications. *Alp Bot*. 2017;127(1):1–15.
57. Feng Y, Ziegler AD, Elsen PR, Liu Y, He X, Spracklen DV, Holden J, Jiang X, Zheng C, Zeng Z. Upward expansion and acceleration of forest clearance in the mountains of Southeast Asia. *Nat Sustain*. 2021;4(10):892–899.
58. Zeng Z, Gower DB, Wood EF. Accelerating forest loss in southeast Asian massif in the 21st century: A case study in Nan Province. *Thailand Glob Chang Biol*. 2018;24(10):4682–4695.
59. Li P, Feng Z, Jiang L, Liao C, Zhang J. A review of swidden agriculture in Southeast Asia. *Remote Sens*. 2014;6(2):1654–1683.
60. Buchner J, Yin H, Frantz D, Kuemmerle T, Askerov E, Bakuradze T, Bleyhl B, Elizbarashvili N, Komarova A, Lewińska KE, et al. Land-cover change in the Caucasus Mountains since 1987 based on the topographic correction of multi-temporal Landsat composites. *Remote Sens Environ*. 2020;248:111967.
61. Breiman L. Random forests. *Mach Learn*. 2001;45(1):5–32.
62. Lang N, Walter Jetz KS, Jan Dirk Wegner. A high-resolution canopy height model of the Earth. ArXiv 2022. arXiv:2204.08322.

63. Mohajane M, Costache R, Karimi F, Pham QB, Essahlaoui A, Nguyen H, Laneve G, Oudija F. Application of remote sensing and machine learning algorithms for forest fire mapping in a Mediterranean area. *Ecol Indic*. 2021;129:107869.
64. Rogan J, Franklin J, Stow D, Miller J, Woodcock C, Roberts D. Mapping land-cover modifications over large areas: A comparison of machine learning algorithms. *Remote Sens Environ*. 2008;112(5):2272–2283.
65. Shelestov A, Lavreniuk M, Kussul N, Novikov A, Skakun S. Exploring Google earth engine platform for big data processing: Classification of multi-temporal satellite imagery for crop mapping. *Front Earth Sci*. 2017;5:17.
66. Pelletier C, Valero S, Inglada J, Champion N, Dedieu G. Assessing the robustness of random forests to map land cover with high resolution satellite image time series over large areas. *Remote Sens Environ*. 2016;187:156–168.
67. Rouse JW Jr, Haas RH, Schell JA, Deering DW. Monitoring the vernal advancement and retrogradation (green wave effect) of natural vegetation (no. NASA-CR-132982). 1973.
68. Allouche O, Tsoar A, Kadmon R. Assessing the accuracy of species distribution models: Prevalence, kappa and the true skill statistic (TSS). *J Appl Ecol*. 2006;43(6):1223–1232.
69. Lewis H, Brown M. A generalized confusion matrix for assessing area estimates from remotely sensed data. *Int J Remote Sens*. 2001;22(16):3223–3235.
70. Olofsson P, Foody GM, Herold M, Stehman SV, Woodcock CE, Wulder MA. Good practices for estimating area and assessing accuracy of land change. *Remote Sens Environ*. 2014;148:42–57.
71. Stehman SV, Foody GM. Key issues in rigorous accuracy assessment of land cover products. *Remote Sens Environ*. 2019;231:111199.
72. Fox J, Castella JC, Ziegler AD, Westley SB. Expansion of rubber mono-cropping and its implications for the resilience of ecosystems in the face of climate change in Montane Mainland Southeast Asia; 2014.
73. Balzter H, Rowland CS, Saich P. Forest canopy height and carbon estimation at monks Wood National Nature Reserve, UK, using dual-wavelength SAR interferometry. *Remote Sens Environ*. 2007;108(3):224–239.
74. Hansen MC, Stehman SV, Potapov PV. Quantification of global gross forest 421 cover loss. *Proc Natl Acad Sci U S A*. 2010;107:8650–8655.
75. Bastin JF, Berrahmouni N, Grainger A, Maniatis D, Mollicone D, Moore R, Patriarca C, Picard N, Sparrow B, Abraham EM, et al. The extent of forest in dryland biomes. *Science*. 2017;356(6338):635–638.
76. Brandt M, Tucker CJ, Kariryaa A, Rasmussen K, Abel C, Small J, Chave J, Rasmussen LV, Hiernaux P, Diouf AA, et al. An unexpectedly large count of trees in the west African Sahara and Sahel. *Nature*. 2020;587(7832):78–82.
77. Ge Y, Chen Y, Li S, Jiang Y. Vectorial boundary-based sub-pixel mapping method for remote-sensing imagery. *Int J Remote Sens*. 2014;35(5):1756–1768.
78. Wilcove DS, Giam X, Edwards DP, Fisher B, Koh LP. Navjot's nightmare revisited: Logging, agriculture, and biodiversity in Southeast Asia. *Trends Ecol Evol*. 2013;28:531–540.
79. Palmer C. The extent and causes of illegal logging: An analysis of a major cause of tropical deforestation in Indonesia (CSERGE Working Papers). London, UK: Centre for Social and Economic Research on the Global Environment (CSERGE); 2001.
80. White JC, Hermosilla T, Wulder MA, Coops NC. Mapping, validating, and interpreting spatio-temporal trends in post-disturbance forest recovery. *Remote Sens Environ*. 2022;271:112904.
81. Zhu X, Liu D. Accurate mapping of forest types using dense seasonal Landsat time-series. *ISPRS J Photogramm Remote Sens*. 2014;96:1–11.
82. Singha M, Dong J, Zhang G, Xiao X. High resolution paddy rice maps in cloud-prone Bangladesh and Northeast India using Sentinel-1 data. *Sci Data*. 2019;6(1):1–10.
83. Xu L, Herold M, Tsendbazar NE, Masiliūnas D, Li L, Lesiv M, Fritz S, Verbesselt J. Time series analysis for global land cover change monitoring: A comparison across sensors. *Remote Sens Environ*. 2022;271:112905.
84. Naesset E, Ørka HO, Solberg S, Bollandsås OM, Hansen EH, Mauya E, Zahabu E, Malimbwi R, Chamuya N, Olsson H, et al. Mapping and estimating forest area and aboveground biomass in miombo woodlands in Tanzania using data from airborne laser scanning, TanDEM-X, RapidEye, and global forest maps: A comparison of estimated precision. *Remote Sens Environ*. 2016;175:282–300.
85. Ringrose S, Matheson W, Mogotsi B, Tempest F. The darkening effect in drought affected savanna woodland environments relative to soil reflectance in Landsat and SPOT wavebands. *Remote Sens Environ*. 1989;30(1):1–19.
86. Hermosilla T, Wulder MA, White JC, Coops NC. Land cover classification in an era of big and open data: Optimizing localized implementation and training data selection to improve mapping outcomes. *Remote Sens Environ*. 2022;268:112780.
87. Yulianto F, Nugroho G, Aruba Chulafak G, Suwarsono S. Improvement in the accuracy of the postclassification of land use and land cover using landsat 8 data based on the majority of segment-based filtering approach. *Sci World J*. 2021.
88. Zapata-Rios X, Brooks PD, Troch PA, McIntosh J, Guo Q. Influence of terrain aspect on water partitioning, vegetation structure and vegetation greening in high-elevation catchments in northern New Mexico. *Ecohydrology*. 2016;9(5):782–795.
89. McCarthy MJ, Jessen B, Barry MJ, Figueroa M, McIntosh J, Murray T, Schmid J, Muller-Karger FE. Automated high-resolution time series mapping of mangrove forests damaged by hurricane Irma in Southwest Florida. *Remote Sens*. 2020;12(11):1740.
90. Meng S, Pang Y, Huang C, Li Z. Improved forest cover mapping by harmonizing multiple land cover products over China. *GIsci Remote Sens*. 2022;59(1): 1570–1597.
91. Archibald S, Bond WJ, Hoffmann W, Lehmann C, Staver C, Stevens N. *Distribution and determinants of savannas.* In: *Savanna woody plants and large herbivores.* Hoboken (NJ): John Wiley & Sons Ltd.; 2019.